

Generating Optimal Grasps Under A Stress-Minimizing Metric

Zherong Pan¹, Xifeng Gao², and Dinesh Manocha³

Abstract—We present stress-minimizing (SM) metric, a new metric of grasp qualities. Unlike previous metrics that ignore the material of target objects, we assume that target objects are made of homogeneous isotropic materials. SM metric measures the maximal resistible external wrenches without causing fracture in the target objects. Therefore, SM metric is useful for robot grasping valuable and fragile objects. In this paper, we analyze the properties of this new metric, propose grasp planning algorithms to generate globally optimal grasps maximizing the SM metric, and compare the performance of the SM metric and a conventional metric. Our experiments show that SM metric is aware of the geometries of target objects while the conventional metric are not. We also show that the computational cost of the SM metric is on par with that of the conventional metric.

I. INTRODUCTION

The performance and properties of (asymptotically) optimal grasp planning algorithms heavily depend on the type of grasp quality metrics. A summary of these metrics can be found in [18]. Usual requirements for a good grasp include: force closure, small contact force magnitudes, the preference of normal forces over frictional forces, higher resilience to external wrenches. The type of a metric not only reflects the requirements of an application, but also incurs different planning algorithms. For example, the $Q_{1,\infty}$ metrics are submodular, which allows fast discrete grasp point selection [19]. The Q_1 metric has an optimizable lower-bound, which allows an optimization-based grasp planning algorithm [6] to jointly search for grasp points and grasp poses.

However, all the metrics considered so far take a common assumption about the target object: these objects are of infinite stiffness and will never be broken. As a result, we can assume that the target object is a rigid body and all the forces and torques are applied on the center-of-mass, which greatly simplify the computation and analysis of metrics. However, this assumption does not hold when grasping fragile objects where certain weak parts of an object should not be touched to avoid possible fractures. The grasp of fragile objects have been considered in prior works [16], [1], which attempt to avoid breaking objects by developing safer grippers. Instead, we argue that, in addition to better robot hardware, a new metric is needed to guide the grasp planning algorithm, so that we can find a grasp that is most unlikely to break the object.

Main Results: We present a novel metric that relaxes the infinite stiffness assumption and takes the material of

the target object into consideration. Based on the theory of brittle fracture [9], we formulate the set of external wrenches that can be resisted without causing fractures in the object. Similar to the Q_1 metric [7], [19], our metric then measures the size of the space of resistible wrenches. We call this new metric stress-minimizing (SM) metric Q_{SM} . We show that, using boundary element method (BEM) [5], Q_{SM} can be computed efficiently, given a closed surface triangle mesh of the object and a set of contact points. The cost of computing Q_{SM} is on par with that of computing Q_1 . In addition, we show that conventional optimization-based grasp planning algorithms [19] can be modified to search for globally optimal grasps maximizing Q_{SM} .

The rest of the paper is organized as follows. We review related work in Section VI and formulation the problem of grasp planning in Section III. The formulation of Q_{SM} and its properties are summarized in Section IV. Grasp planning algorithms using Q_{SM} as metric are formulated in Section V. Finally, we compare Q_{SM} with conventional metric Q_1 in Section VI.

II. RELATED WORK

We review related work in grasp quality metric, material and fracture modeling, and grasp planning.

Grasp Quality Metric: Although some grasp planners only consider external wrenches along some certain directions [15], more prominent characterization of robust grasp requires resilience to external wrenches along all directions, which is known as force closure [17]. However, infinitely many grasps can have force closure, of which good grasps are characterized by different quality metrics [18]. Most of the metrics Q are designed such that $Q > 0$ implies force closure. A closely related metric to our Q_{SM} is $Q_{1,\infty}$ [7], which measures the maximal radius of origin-centered wrench-space circle contained in the convex set of resistible wrenches, under contact force magnitude constraints.

Material and Fracture Modeling: Real world solid objects will undergo either brittle or ductile fractures depending on their materials. But modeling them are both theoretically and computationally difficult [9]. Fortunately, for grasp planning, we do not need to model the deformation of objects after fractures, but only need to detect where fractures might happen. In this case, the theory of linear elasticity suffices, which is efficient to compute using finite element method (FEM) [13] or boundary element method (BEM) [5]. We use BEM as our computational tool because it only requires a surface triangle mesh which is more amenable to robot grasp applications.

Grasp Planning: Given a grasp quality metric, an (asymptotically) optimal grasp planning algorithm finds a grasp that maximizes the grasp quality metric. Early algorithms [22]

¹Zherong is with Department of Computer Science, University of North Carolina at Chapel Hill. {zherong@cs.unc.edu}

²Xifeng Gao is with Department of Computer Science, Florida State University. {gao@cs.fsu.edu}

³Dinesh Manocha is with Department of Computer Science and Electrical & Computer Engineering, University of Maryland at College Park. {dm@cs.umd.edu}

use sampling-based methods for planning. These algorithms are very general and they are agnostic to the type of grasp quality metrics. However, more efficient algorithms such as [6], [19] can be designed if quality metrics have certain properties. Recent work [14] uses a set of precomputed quality metrics to train a grasp quality function represented by a deep neural network and then uses the function as reward to optimize a grasp planner via deep reinforcement learning.

III. PROBLEM STATEMENT

In this section, we formulate the problem of stress-minimizing grasp planning. Throughout the paper, we keep a 3D target object in its reference space, where the origin coincides with its center-of-mass. The object takes up a volume which is a closed subset $\Omega \subset R^3$. In addition, the object is under an external 6D wrench \mathbf{w} and a set of N external contact forces $\mathbf{f}_1, \dots, \mathbf{f}_N$ at contact points $\mathbf{x}_1, \dots, \mathbf{x}_N$ with unit contact normals $\mathbf{n}_1, \dots, \mathbf{n}_N$. If a grasp is valid, we have the following wrench balance condition:

$$\mathbf{w} = - \sum_{i=1}^N \begin{pmatrix} \mathbf{f}_i \\ \mathbf{x}_i \times \mathbf{f}_i \end{pmatrix} \quad \text{s.t.} \quad \|(\mathbf{I} - \mathbf{n}_i \mathbf{n}_i^T) \mathbf{f}_i\| \leq \theta \mathbf{n}_i^T \mathbf{f}_i, \quad (1)$$

where θ is the frictional coefficient. To compare the quality of two different grasps, a well-known method is to compare their Q_1 metric [7], which is the maximal radius of the origin-centered inscribed sphere in the convex hull of all possible resistible external wrenches when the magnitude of \mathbf{f}_i is bounded. Mathematically, this is:

$$Q_1 = \mathbf{max} r \quad \text{s.t.} \{ \mathbf{w} | \mathbf{w}^T \mathbb{W} \mathbf{w} \leq r^2 \} \subseteq \{ \mathbf{w} | \exists \mathbf{f}_1, \dots, \mathbf{f}_N, \text{ s.t. Equation 1, } \sum_{i=1}^N \|\mathbf{f}_i\|^2 \leq 1 \},$$

where \mathbb{W} is the 6×6 positive semi-definite metric tensor in the wrench space.

However, this conventional formulation assumes that the object will never be broken however large the external forces are. To relax this condition, we have to make use of the numerical models of brittle fracture, e.g. [9]. In these formulations, we assume that the object is made of homogeneous isotropic elastic material with λ, μ being its Lamé material parameters. When under external force fields $\mathbf{g}(\mathbf{x}) : R^3 \rightarrow R^3$, an infinitesimal displacement $\mathbf{u}(\mathbf{x}) : R^3 \rightarrow R^3$ and an stress field $\boldsymbol{\sigma}(\mathbf{x}) : R^3 \rightarrow R^{3 \times 3}$ will occur $\forall \mathbf{x} \in \Omega$. $\mathbf{u}(\mathbf{x}), \boldsymbol{\sigma}(\mathbf{x})$ can be computed from $\mathbf{g}(\mathbf{x})$ using the force balance condition:

$$\begin{aligned} \forall \mathbf{x} \in \Omega : \quad & \boldsymbol{\epsilon} = (\nabla \mathbf{u} + \nabla \mathbf{u}^T) / 2 \\ & \boldsymbol{\sigma} = 2\mu \boldsymbol{\epsilon} + \lambda \text{tr}(\boldsymbol{\epsilon}) \mathbf{I} \\ & \nabla \cdot \boldsymbol{\sigma} + \mathbf{g} = 0 \end{aligned} \quad (2)$$

$$\forall \mathbf{x} \in \partial\Omega : \quad \mathbf{n}(\mathbf{x}) \cdot \boldsymbol{\sigma} + \sum_{i=1}^N \delta(\mathbf{x} - \mathbf{x}_i) \mathbf{f}_i = 0,$$

where we assume the boundary of Ω is almost everywhere smooth with unit outward normal defined as $\mathbf{n}(\mathbf{x})$ and δ is the Dirac's delta operator. Classical theory of brittle fracture further assumes that there exists a tensile stress σ_{max} and brittle fractures will not happen if the following condition

holds:

$$\forall \|\mathbf{d}\| = 1, \mathbf{x} \in \Omega : \quad -\sigma_{max} \leq \mathbf{d}^T \boldsymbol{\sigma}(\mathbf{x}) \mathbf{d} \leq \sigma_{max}, \quad (3)$$

note that the stress tensor must be symmetric so that its singular values coincide with its eigenvalues. Given this condition, there are two goals of this paper:

- Propose a grasp quality metric Q_{SM} that measures the quality of grasps with Equation 3 as precondition (Section IV).
- Propose grasp planning algorithms that generate grasps maximizing Q_{SM} (Section V).

IV. THE STRESS-MINIMIZING METRIC Q_{SM}

Our construction is illustrated in Figure 1. The basic idea behind the construction of Q_{SM} is very similar with that of the Q_1 metric. Intuitively, we first define a convex subset \mathbf{W} of the 6D wrench space, which contains resistible wrenches that does not violate Equation 3. We then define Q_{SM} as the maximal radius of the origin-centered sphere contained in \mathbf{W} .

A. Definition of \mathbf{W} and Q_{SM}

Given a certain wrench \mathbf{w} , we need to determine whether $\mathbf{w} \in \mathbf{W}$. This can be done by first computing $\boldsymbol{\sigma}$ and then testing whether Equation 3 holds. However, $\boldsymbol{\sigma}$ is computed from \mathbf{g} but not \mathbf{w} , so that we need to find a relationship between \mathbf{g} and \mathbf{w} . In other words, we need to find a body force distribution such that the net effect of \mathbf{g} is equivalent to applying \mathbf{w} on the center-of-mass. Obviously, infinitely many \mathbf{g} will satisfy this relationship and different choices of \mathbf{g} will lead to different variants of Q_{SM} metrics. In this paper, we propose to choose \mathbf{g} as a linear function in \mathbf{x} . The most important reason behind this choice is that the computation of $\boldsymbol{\sigma}$ can be accomplished using BEM if \mathbf{g} is a harmonic function of \mathbf{x} . Under this choice, we have: $\mathbf{g}(\mathbf{x}) = \mathbf{g}_0 + \nabla \mathbf{g} \mathbf{x}$, where \mathbf{g}_0 is the constant term, $\nabla \mathbf{g}$ is the constant spatial derivative tensor. Clearly $\mathbf{g}(\mathbf{x})$ has 12 degrees of freedom and we can solve for \mathbf{g}_0 and $\nabla \mathbf{g}$ to equate the effect of \mathbf{g} and \mathbf{w} as follows:

$$\mathbf{w} = \int_{\Omega} \begin{pmatrix} \mathbf{g} \\ \mathbf{x} \times \mathbf{g} \end{pmatrix} d\mathbf{x} = \begin{pmatrix} |\Omega| \mathbf{g}_0 \\ \mathcal{T} \begin{pmatrix} [\nabla \mathbf{g}]_x \\ [\nabla \mathbf{g}]_y \\ [\nabla \mathbf{g}]_z \end{pmatrix} \end{pmatrix}$$

$$\mathcal{T} \triangleq \int_{\Omega} (x \mathbf{x} \times y \mathbf{x} \times z \mathbf{x} \times) d\mathbf{x},$$

where $[\nabla \mathbf{g}]_{x,y,z}$ are the first, second, and third column of $\nabla \mathbf{g}$, respectively. However, there are 9 degrees of freedom in \mathbf{g}_x but only 3 constraints, so that we have to solve for \mathbf{g}_x in a least square sense:

$$\mathbf{g}_x = \mathbf{argmin}_{\mathbf{g}_x} \int_{\Omega} \|\mathbf{g}_x \mathbf{x}\|^2 d\mathbf{x} \quad \text{s.t.} \quad \mathcal{T} \begin{pmatrix} [\nabla \mathbf{g}]_x \\ [\nabla \mathbf{g}]_y \\ [\nabla \mathbf{g}]_z \end{pmatrix} = \begin{pmatrix} \mathbf{w}_4 \\ \mathbf{w}_5 \\ \mathbf{w}_6 \end{pmatrix},$$

the solution of which can be computed analytically. In summary, we have:

$$\begin{pmatrix} \mathbf{g}_0 \\ [\nabla \mathbf{g}]_x \\ [\nabla \mathbf{g}]_y \\ [\nabla \mathbf{g}]_z \end{pmatrix} = \begin{pmatrix} \mathbf{I} \\ |\Omega| \end{pmatrix} \mathcal{M}^{-1} \mathcal{T}^T [\mathcal{T} \mathcal{M}^{-1} \mathcal{T}^T]^{-1} \mathbf{w} \quad (4)$$

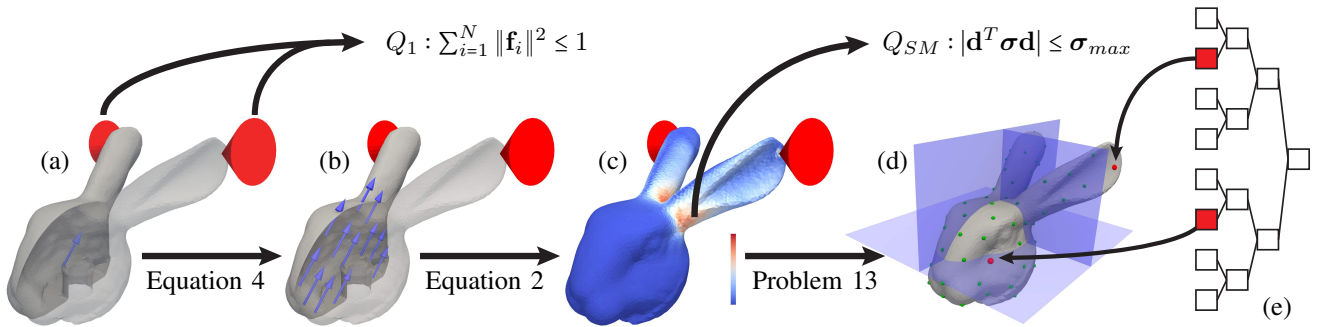


Fig. 1: Illustration of our method where the target object is a bunny head and the two-point grasp has contact points on the ears of bunny (frictional cones in red). (a): When the bunny head is under external wrench (blue arrow), Q_1 metric assumes that the wrench is applied on the center-of-mass. Q_1 further assumes that the magnitude of force is bounded. (b): Our Q_{SM} metric assumes that the external wrench is applied as a body force field (blue arrows). (c): We use BEM to solve for a surface stress field (color coded on surface, highest stress around connections between the ears and the head). Q_{SM} assumes that the stress along any direction \mathbf{d} is smaller than tensile stress σ_{max} . (d): When performing grasp planning, we first construct a KD-tree (transparent blue planes) for the set of N potential contact points. (e): We select C contact points (red points) by descending the tree. This is equivalent to a mixed-integer programming problem with $\log_2(N)C$ binary decision variables.

$$\mathcal{M} \triangleq \left[\int_{\Omega} \mathbf{x} \mathbf{x}^T dx \right] \otimes \mathbf{I},$$

where \otimes denotes Kronecker product. The matrices \mathcal{T}, \mathcal{M} are constants and can be precomputed from the shape of the target object, or more specifically, from the inertia tensor. Given these definitions, we can now define \mathbf{W} as follows:

$$\mathbf{W} = \{ \mathbf{w} | \exists \mathbf{g}, \mathbf{f}_1, \dots, \mathbf{f}_N, \mathbf{u}, \boldsymbol{\epsilon}, \boldsymbol{\sigma}, \text{ s.t. } \text{Equation 1, 2, 3, 4} \}. \quad (5)$$

Finally, we are ready to give a mathematical definition of Q_{SM} as the following optimization problem:

$$Q_{SM} = \max r \quad \text{s.t.} \quad \{ \mathbf{w} | \mathbf{w}^T \mathbb{W} \mathbf{w} \leq r^2 \} \subseteq \mathbf{W}.$$

From the mathematical definition of Q_{SM} , we immediately have the following properties of \mathbf{W} :

Lemma 4.1: \mathbf{W} is a convex set.

Proof: Equation 1 is a set of quadratic cone constraints, which defines a convex set. Equation 2 is a set of infinite-dimensional linear constraints, which defines a convex set. Equation 3 is an infinite-dimensional PSD-cone constraint, which defines a convex set. Finally, Equation 4 is a linear constraint, which also defines a convex set. As the intersection of convex sets, \mathbf{W} is convex. ■

Lemma 4.2: \mathbf{W} is a compact set so that Q_{SM} is finite.

Proof: For any $\mathbf{w} \neq 0$, $\boldsymbol{\sigma}$ that satisfies Equation 1, Equation 2, and Equation 4 cannot be uniformly zero. In other words, there exists \mathbf{d} and \mathbf{x} such that $\mathbf{d}^T \mathbf{u}(\mathbf{x}) \mathbf{d} > \epsilon > 0$. If we multiply \mathbf{w} by $\alpha > \sigma_{max}/\epsilon$, Equation 3 will be violated so that $\alpha \mathbf{w} \notin \mathbf{W}$. Therefore, \mathbf{W} is bounded and is obviously closed, so that \mathbf{W} is compact and Q_{SM} is finite. ■

In addition, the following property of Q_{SM} is obvious:

Lemma 4.3: $Q_{SM} > 0$ implies force closure.

And the following property has been proved in [19] for Q_1 and also holds for Q_{SM} by a similar argument:

Lemma 4.4: $Q_{SM} = \min_{\mathbf{d}, \|\mathbf{d}\|=1} \max_{\mathbf{w} \in \sqrt{\mathbb{W}}} \mathbf{w}^T \mathbf{d}$.

B. Discretization of Q_{SM}

The computation of exact Q_{SM} is impossible because it involves infinite dimensional tensor fields: $\boldsymbol{\sigma}, \boldsymbol{\epsilon}$, so that we

have to discretize them using conventional techniques such as FEM [13] or BEM [5]. In comparison, FEM is mathematically simpler but requires a volumetric mesh of the target object, while BEM only requires a surface triangle mesh. We provide the detailed derivation of BEM in Appendix and summarize the main results here. Our BEM implementation approximates the stress field $\boldsymbol{\sigma}(\mathbf{x})$ to be piecewise constant on each triangular patch of the surface. Assuming that the target object has K surface triangles whose centroids are: $\mathbf{x}_1, \dots, \mathbf{x}_K$, we have K different stress values:

$$\begin{pmatrix} \sigma_x(\mathbf{x}_j) \\ \sigma_y(\mathbf{x}_j) \\ \sigma_z(\mathbf{x}_j) \end{pmatrix} = \mathcal{A}_j \begin{pmatrix} \mathbf{g}_0 \\ [\nabla \mathbf{g}]_x \\ [\nabla \mathbf{g}]_y \\ [\nabla \mathbf{g}]_z \end{pmatrix} + \mathcal{B}_j \begin{pmatrix} \mathbf{f}_1 \\ \vdots \\ \mathbf{f}_N \end{pmatrix} \quad \forall j = 1, \dots, K, \quad (6)$$

where \mathcal{A}, \mathcal{B} are dense coefficient matrices defined from BEM discretization, the definitions of which can be found from Appendix . Note that computing the coefficients of these two matrices are very computationally costly, where a naive implementation of BEM requires $\mathcal{O}(K^3)$ operations and acceleration techniques such as the H-matrix [11] can reduce this cost to $\mathcal{O}(K \log^2 K)$ operations. However, these two matrices are constant and can be precomputed for a given target object shape, so that the cost of BEM computation is not a part of grasp planning. After discretization, we arrive at the finite-dimensional version of fracture condition:

$$\forall \|\mathbf{d}\| = 1, j = 1, \dots, K : -\sigma_{max} \leq \mathbf{d}^T \boldsymbol{\sigma}(\mathbf{x}_j) \mathbf{d} \leq \sigma_{max}. \quad (7)$$

finite-dimensional version of $\bar{\mathbf{W}}$:

$$\bar{\mathbf{W}} \triangleq \{ \mathbf{w} | \exists \mathbf{g}, \mathbf{f}_1, \dots, \mathbf{f}_N, \mathbf{u}, \boldsymbol{\epsilon}, \boldsymbol{\sigma}, \text{ s.t. } \text{Equation 1, 6, 7, 4} \},$$

and finite-dimensional version of Q_{SM} defined as:

$$\bar{Q}_{SM} = \arg \max r \quad \text{s.t.} \quad \{ \mathbf{w} | \mathbf{w}^T \bar{\mathbb{W}} \mathbf{w} \leq r^2 \} \subseteq \bar{\mathbf{W}}.$$

All the properties of the infinite-dimensional \mathbf{W} and Q_{SM} hold for the finite-dimensional version $\bar{\mathbf{W}}$ and \bar{Q}_{SM} by a similar argument.

C. Computation of \bar{Q}_{SM}

Even after discretization, computing \bar{Q}_{SM} is costly and non-trivial. According to Lemma 4.4, the equivalent optimization problem for \bar{Q}_{SM} is:

$$\bar{Q}_{SM} = \min_{\mathbf{d}, \|\mathbf{d}\|=1} \max_{\mathbf{w} \in \sqrt{\mathbb{W}}\bar{\mathbb{W}}} \mathbf{w}^T \mathbf{d},$$

which is non-convex optimization, so that direct optimization does not give the global optimum. In this section, we modify three existing algorithms to (approximately) compute \bar{Q}_{SM} . Two discrete algorithms have been proposed in [23], [19] to approximate Q_1 . Due to the close relationships between Q_1 and \bar{Q}_{SM} , we show that these two algorithms can be modified to compute \bar{Q}_{SM} .

In [19], the space of unit vectors is discretized into a finite set of D directions: $\mathbf{d}_1, \dots, \mathbf{d}_D$. As a result, we can compute an upper bound for \bar{Q}_{SM} as:

$$\bar{Q}_{SM} \leq \min_{j=1, \dots, D} \max_{\mathbf{w} \in \sqrt{\mathbb{W}}\bar{\mathbb{W}}} \mathbf{w}^T \mathbf{d}_j.$$

We can make this upper bound arbitrarily tight by increasing D . In another algorithm [23], a convex polytope $\mathcal{C} \subseteq \bar{\mathbb{W}}$ is maintained using H-representation [10] and we can compute a lower bound for \bar{Q}_{SM} as:

$$\bar{Q}_{SM} \geq \min_{\mathbf{d}, \|\mathbf{d}\|=1} \max_{\mathbf{w} \in \sqrt{\mathbb{W}}\bar{\mathbb{C}}} \mathbf{w}^T \mathbf{d}. \quad (8)$$

The global optimum of Problem 8 is easy to compute from an H-representation of \mathcal{C} by computing the distance between the origin and each face of \mathcal{C} . This lower bound can be iteratively tightened by first computing the blocking face normal \mathbf{d} of \mathcal{C} and then expanding \mathcal{C} via:

$$\mathcal{C} \leftarrow \text{ConvexHull}(\mathcal{C} \cup \left\{ \underset{\mathbf{w} \in \sqrt{\mathbb{W}}\bar{\mathbb{W}}}{\text{argmax}} \mathbf{w}^T \mathbf{d} \right\}).$$

These two algorithms can be realized if we can find the supporting point of $\sqrt{\mathbb{W}}\bar{\mathbb{W}}$, which amounts to the following conic programming problem:

$$\begin{aligned} & \underset{\mathbf{w}, \mathbf{f}_i, \sigma(\mathbf{x}_j)}{\text{argmax}} \mathbf{w}^T \sqrt{\mathbb{W}}\mathbf{d} \\ & \text{s.t. Equation 1, 6, 4} \end{aligned} \quad (9)$$

$$- \sigma_{max} \mathbf{I} \leq \sigma(\mathbf{x}_j) \leq \sigma_{max} \mathbf{I} \quad \forall j = 1, \dots, K.$$

The conic programming reformulation in Problem 9 can be solved using the interior point method [3]. Given this solution procedure, we summarize the modified version of [19] in Algorithm 1 and modified version of [23] in Algorithm 2. Note that Algorithm 2 is advantageous over Algorithm 1 in that it can approximate \bar{Q}_{SM} up to arbitrary precision ϵ , so we always use Algorithm 2 in the rest of the paper.

Compared with Q_1 metric, a major limitation of using \bar{Q}_{SM} metric is that the computational cost is much higher. Note that the computational cost of solving Problem 9 is at least linear in K and can be superlinear depending on the type of conic programming solver used. This K is the number of surface triangles on the target object, which can easily reach several thousands. Fortunately, we can drastically reduce this cost by using a progressive approach.

D. Performance Optimization

The naive execution of Algorithm 2 can be prohibitively slow due to the repeated solve of Problem 9. The conic

programming problem has K PSD-cone constraints with K being several thousands. Solving Problem 9 using interior point method [3] involves repeated solving a sparse linear system with size proportional to K . We propose a method that can greatly improve the performance when solving Problem 9. Our idea is that when the global optimum of Problem 9 is reached, more than 99% of the K PSD-cone constraints are inactive, so that removing these constraints do not alter the solution. This idea is inspired by [24] which shows that, empirically, maximal stress only happens on a few sparse points on the surface of the target object. However, we do not know the active constraints as a prior. Therefore, we propose to progressively detect these active constraints.

To do so, we first select a subset $\mathbb{K} \subset \{1, \dots, K\}$ such that $|\mathbb{K}| \ll K$ and $\{\sigma(\mathbf{x}_i) | i \in \mathbb{K}\}$ are the stresses that are most likely to be violated. To select this set \mathbb{K} , we use a precomputation step and solve Problem 9 for S times using random \mathbf{d} , and record which PSD-cones are active. For each PSD-cone, we maintain how many times they become active during the S solves of Problem 9. We then select the most frequent $|\mathbb{K}|$ PSD-cones to form \mathbb{K} . After selecting \mathbb{K} , we maintain an active set \mathcal{S} which initializes to \mathbb{K} and we solve Problem 9 using constraints only in \mathcal{S} , which is denoted by:

$$\begin{aligned} & \underset{\mathbf{w}, \mathbf{f}_i, \sigma(\mathbf{x}_j)}{\text{argmax}} \mathbf{w}^T \sqrt{\mathbb{W}}\mathbf{d} \\ & \text{s.t. Equation 1, 6, 4} \end{aligned} \quad (10)$$

$$- \sigma_{max} \mathbf{I} \leq \sigma(\mathbf{x}_j) \leq \sigma_{max} \mathbf{I} \quad \forall j \in \mathcal{S}.$$

After we solve for the global optimum of Problem 10, we check the stress of remaining constraint points and we pick the most violated constraint:

$$j^* = \underset{j \in \{1, \dots, K\} / \mathcal{S}}{\text{argmax}} \sqrt{\|\sigma(\mathbf{x}_j) \sigma(\mathbf{x}_j)\|_2}. \quad (11)$$

If we have $\sqrt{\|\sigma(\mathbf{x}_{j^*}) \sigma(\mathbf{x}_{j^*})\|_2} < \sigma_{max}$, then Problem 10 and Problem 9 will return the same solution. Otherwise, we add j^* to \mathcal{S} . This method is summarized in Algorithm 3 and is guaranteed to return the same global optimum of Problem 9. In practice, Algorithm 3 is orders of magnitude more efficient than throwing all constraints to the interior point method at once.

V. GRASP PLANNING UNDER THE SM METRIC

Built on top of the computational procedure of \bar{Q}_{SM} , we can solve the optimal grasp point selection problem. Given a set of N potential grasp points sampled on $\partial\Omega$, we want to select C points. Mathematically, we want to solve the following mixed-integer optimization problem using branch-and-bound (BB) algorithm [4]:

$$\begin{aligned} & \underset{z_i}{\text{argmax}} \bar{Q}_{SM} \\ & \text{s.t. } z_i \in \{0, 1\} \quad \forall i = 1, \dots, N \\ & \quad \|\mathbf{f}_i\|^2 \leq z_i M \wedge \sum_{i=1}^N z_i \leq C, \end{aligned} \quad (12)$$

where M is the big-M constant that can be arbitrarily large. Note that the algorithm to solve Problem 12 can be different depending on what algorithm we use to (approximately)

compute \bar{Q}_{SM} . If approximate Algorithm 1 is used, then the problem can be efficiently solved using the sub-modular coverage algorithm [19]. However, in order to highlight the advantage of our new metric, we would like to compute \bar{Q}_{SM} accurately using Algorithm 2. In Section V-A, we show that Problem 12 can be solved a lot more efficiently using a series of reformulations, without changing the global optimum.

A. Optimized BB Algorithm

Our key innovation is via the following reformulation:

$$\begin{aligned} & \underset{z_i^j}{\operatorname{argmax}} \bar{Q}_{SM} \\ & \text{s.t. } z_i^j \in [0, 1] \quad \forall i = 1, \dots, N \quad j = 1, \dots, C \\ & \|\mathbf{f}_i\|^2 \leq \sum_{j=1}^C z_i^j M \wedge \{z_1^j, \dots, z_N^j\} \in \mathcal{SOS}_1 \\ & z_i^j \leq z_i^{j+1} \quad \forall j = 1, \dots, C-1, \end{aligned} \quad (13)$$

where \mathcal{SOS}_1 is the special-ordered-set-of-type-1 [21], which constrains that only one number in a set can take non-zero value. According to [21], we know that Problem 12 requires N binary variables while Problem 13 requires $\log_2(N)C$ binary variables, which is much fewer as $C \ll N$. Intuitively, Problem 13 build a binary bounding volume hierarchy for the set of N contact points and introduce one binary decision variable for each internal level of the tree to select whether the left or the right child is selected. After a leaf node is reached, a contact point is selected. Finally, the last constraint in Problem 13, $z_i^j \leq z_i^{j+1}$, reflects the order-independence of contact points.

Unfortunately, no optimization tools can solve Problem 13 in an off-the-shelf manner due to the special objective function, so that we develop a special implementation of BB outlined in Algorithm 4. In this algorithm, our binary bounding volume hierarchy is a KD-tree, as illustrated in Figure 1de. The most important component for the efficiency of BB algorithm is the problem relaxation (Line 18) as follows:

$$\bar{Q}_{SM}^{curr} = \max_{\bar{Q}_{SM}} \bar{Q}_{SM} \quad \text{s.t. } \|\mathbf{f}_i\|^2 = 0 \quad \forall i \notin \mathcal{S}, \quad (14)$$

which can be solving using Algorithm 2 by excluding the contact points in \mathcal{S} . We summarize our main results below:

Lemma 5.1: Algorithm 4 returns the global optimum of Problem 13, which is also the global optimum of Problem 12 by setting: $z_i = \sum_{j=1}^C z_i^j$.

Finally, note that all the results in this section hold if we replace Q_{SM} with Q_1 .

VI. EVALUATIONS

We implement our algorithms for computing Q_{SM} and perform grasp planning using C++. The accuracy of BEM heavily relies on the quality of the surface triangle mesh, so that we first optimize the mesh quality using CGAL [2]. We implement the BEM using kernel independent numerical integration scheme [8]. The most computationally costly step in BEM is the inversion of system matrices, for which we use LU-factorization accelerated by H-matrices [11]. Finally, we use CGAL [12] to construct convex hulls with exact

arithmetics. All the experiments are performed on a single desktop machine with two Xeon E5-2697 CPU and 256Gb memory.

Parameter Choices: Computing Q_{SM} requires more parameters than Q_1 . Specifically, there are three additional variables: tensile stress σ_{max} and Lamé material parameters: μ, λ . However, if we transform μ, λ to an equivalent set of parameters: Young's modulus E and Poisson ratio ν [13], it is obvious to show that Q_{SM} is proportional to σ_{max} and inversely proportional to E . Since the absolute value of a grasp metric is meaningless for grasp planning and only the relative value matters, we can always set $\sigma_{max} = E = 1$ and choose only ν according to the material type of the target object, and then setting:

$$\mu = \frac{1}{2(1+\nu)} \quad \lambda = \frac{\nu}{(1+\nu)(1-2\nu)}.$$

We have $\nu = 0.33$ for copper and $\nu = 0.499$ for rubber. In all experiments, we set $\nu = 0.33$. Finally, when running Algorithm 2, we set $\epsilon = 0.001$.

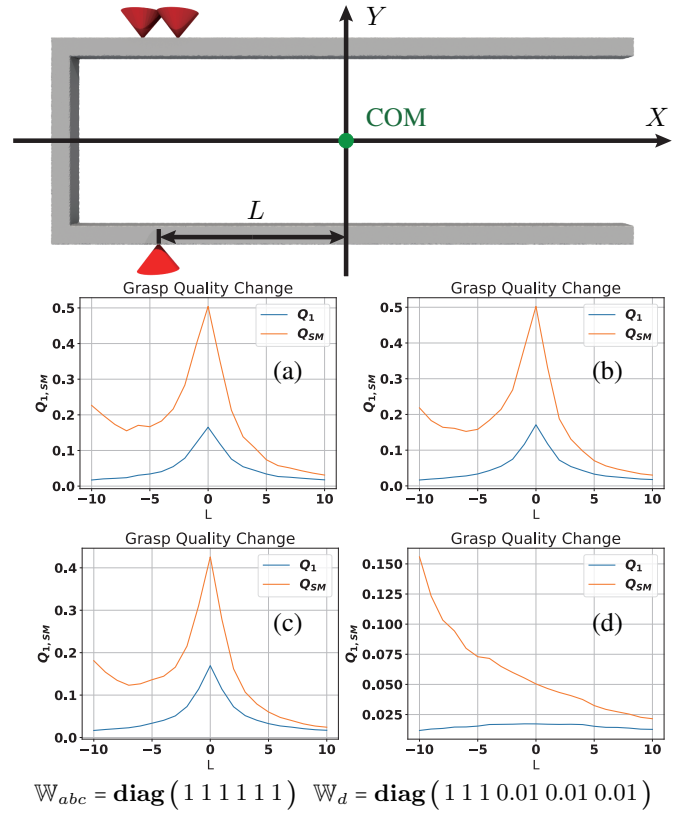


Fig. 2: The target object is a U-shaped tuning fork, where Q_{SM} is aware of shapes while Q_1 is not. We test a 3-point grasp (frictional cones in red) where the distance to the center of mass (green) is L , we plot the change of $Q_{1,SM}$ against L under 4 different conditions. In (a,b,c), we weight forces and torques equally with \mathbb{W}_{abc} and use meshes of different resolutions, with $K = 5730$ in (a), $K = 24204$ in (b), and $K = 94398$ in (c). In (d), we use a lower weight for torques with \mathbb{W}_d and use $K = 24204$.

Shape-Awareness: The most remarkable advantage of

Q_{SM} over Q_1 is shape awareness. In Figure 2, our target object is a U-shaped tuning fork and we use a 3-point grasp. The shape of the tuning fork is asymmetric along the X-axis, and according to Figure 2abc, Q_1 is not aware of the asymmetry, while Q_{SM} correctly reflects the fact that grasping the leftmost point is better than grasping the mid-left point because it is less likely to break the object. However, the best grasp under Q_1 and Q_{SM} are the same, i.e., grasping the centroid point. If we change the metric \mathbb{W} and emphasize force resistance over torque resistance, then the difference between Q_1 and Q_{SM} is more advocated.

Robustness to Mesh Resolution: The change of Q_{SM} is not sensitive to the resolution of surface meshes as shown in Figure 2abc, which makes Q_{SM} robust to target objects discretized using small, low-resolution meshes. As we increase K from 5730 to 24204 and finally to 94398, the change of Q_{SM} against L is almost intact, with very small fluctuations around $L = -5$.

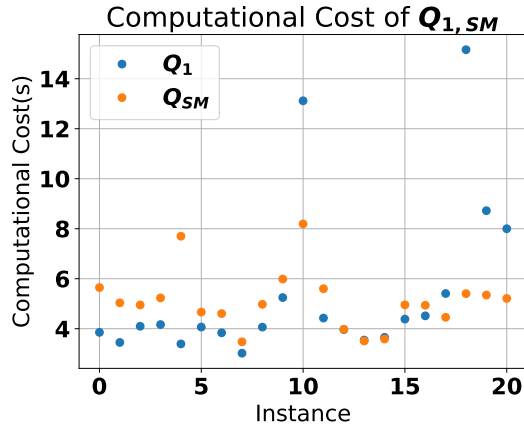


Fig. 3: We compare the computational cost of computing Q_1 and Q_{SM} for 20 random target objects and grasps.

Computational Cost: Q_{SM} does incur a higher computational cost than Q_1 . The most computational cost lies in the assembly of matrices \mathcal{A}, \mathcal{B} which involves the direct factorization of a large dense matrix. But this assembly is precomputation and required only once for each target object before grasp planning. In Figure 2abc, this step takes 112s when $K = 5730$, 1425s when $K = 24204$, and 3892s when $K = 94398$. After precomputation, the cost of evaluating Q_{SM} and Q_1 are very similar, as shown in Figure 3. This implies that using Q_{SM} does not incur a higher cost in grasp planning. This is largely due to the progressive Algorithm 3, which greatly reduce the number of constraints in solving Problem 9. Without this method, solving Problem 9 is prohibitively costly by requiring the solve of a sparse linear system of size proportional to K .

Grasp Planning: In Figure 4, we show globally optimal grasps for 8 different target objects under both the Q_{SM} and Q_1 metric. To generate these results, we choose $C = 3$ contact points from $N = 100$ potential contact points by running Algorithm 4. These contact points are generated using Poisson disk sampling. The computational cost of

Algorithm 4 is 1.7hr under Q_{SM} and 0.6hr under Q_1 on average. This result is surprising as the cost of computing Q_{SM} is comparable to that of computing Q_1 . We found that Q_{SM} tends to create more local minima so that BB needs to create a larger search tree under Q_{SM} . In the third row of Figure 4, we show the maximal stress configuration under Q_1 and the corresponding stress configuration under Q_{SM} side-by-side. The advantage of Q_{SM} is quite clear which suppresses the stress to resist the same external wrench. For some target objects, the high stress is concentrated in a very small region and we indicate them using black circles.

VII. CONCLUSION AND LIMITATION

We present SM metric, which reflects the tendency to break a target object. As a result, a grasp maximizing Q_{SM} will minimize the probability of breaking a fragile object. We show that Q_{SM} can be computed using previous methods and its computational costly can be drastically reduced by progressively detecting the active set. Finally, we show that grasp planning under Q_{SM} can be performed using BB algorithms. Our experiments show that Q_{SM} is aware of geometric fragility while Q_1 is not. We also show that using Q_{SM} does not increase computationally cost in grasp planning.

The major limitation of our work is that computing Q_{SM} requires a costly precomputation step for solving the BEM problem. In addition, the BEM problem requires high quality watertight surface meshes of target objects. An avenue of future research is to infer the value of Q_{SM} for given unknown objects using machine learning, as is done in [14].

REFERENCES

- [1] A. Al-Ibadi, S. Nefti-Meziani, and S. Davis, "Active soft end effectors for efficient grasping and safe handling," *IEEE Access*, vol. 6, pp. 23591–23601, 2018.
- [2] P. Alliez, C. Jamin, L. Rineau, S. Tayeb, J. Tournois, and M. Yvinec, "3D mesh generation," in *CGAL User and Reference Manual*, 4.14 ed. CGAL Editorial Board, 2019.
- [3] E. D. Andersen and K. D. Andersen, "The mosek interior point optimizer for linear programming: an implementation of the homogeneous algorithm," in *High performance optimization*. Springer, 2000, pp. 197–232.
- [4] J. Clausen, "Branch and bound algorithms-principles and examples," 1999.
- [5] T. A. Cruse, D. Snow, and R. Wilson, "Numerical solutions in axisymmetric elasticity," *Computers & Structures*, vol. 7, no. 3, pp. 445–451, 1977.
- [6] H. Dai, A. Majumdar, and R. Tedrake, *Synthesis and Optimization of Force Closure Grasps via Sequential Semidefinite Programming*. Cham: Springer International Publishing, 2018, pp. 285–305.
- [7] C. Ferrari and J. Canny, "Planning optimal grasps," in *Proceedings 1992 IEEE International Conference on Robotics and Automation*, May 1992, pp. 2290–2295 vol.3.
- [8] P. Fiala and P. Rucz, "Nihu: An open source c++ bem library," *Advances in Engineering Software*, vol. 75, pp. 101–112, 2014.
- [9] G. A. Francfort and J.-J. Marigo, "Revisiting brittle fracture as an energy minimization problem," *Journal of the Mechanics and Physics of Solids*, vol. 46, no. 8, pp. 1319–1342, 1998.
- [10] B. Grünbaum and G. C. Shephard, "Convex polytopes," *Bulletin of the London Mathematical Society*, vol. 1, no. 3, pp. 257–300, 1969.
- [11] W. Hackbusch, "A sparse matrix arithmetic based on h-matrices. part i: Introduction to h-matrices," *Computing*, vol. 62, no. 2, pp. 89–108, 1999.
- [12] S. Hert and M. Seel, "dD convex hulls and delaunay triangulations," in *CGAL User and Reference Manual*, 4.14 ed. CGAL Editorial Board, 2019.
- [13] T. J. Hughes, *The finite element method: linear static and dynamic finite element analysis*. Courier Corporation, 2012.
- [14] J. Mahler, J. Liang, S. Niyaz, M. Laskey, R. Doan, X. Liu, J. Aparicio, and K. Goldberg, "Dex-net 2.0: Deep learning to plan robust grasps with synthetic point clouds and analytic grasp metrics," 07 2017.
- [15] J. Mahler, F. T. Pokorny, Z. McCarthy, A. F. van der Stappen, and K. Goldberg, "Energy-bounded caging: Formal definition and 2-d energy lower bound algorithm based on weighted alpha shapes," *IEEE Robotics and Automation Letters*, vol. 1, no. 1, pp. 508–515, 2016.
- [16] B. Matulevich, G. E. Loeb, and J. A. Fishel, "Utility of contact detection reflexes in prosthetic hand control," in *2013 IEEE/RSJ International Conference on Intelligent Robots and Systems*, Nov 2013, pp. 4741–4746.

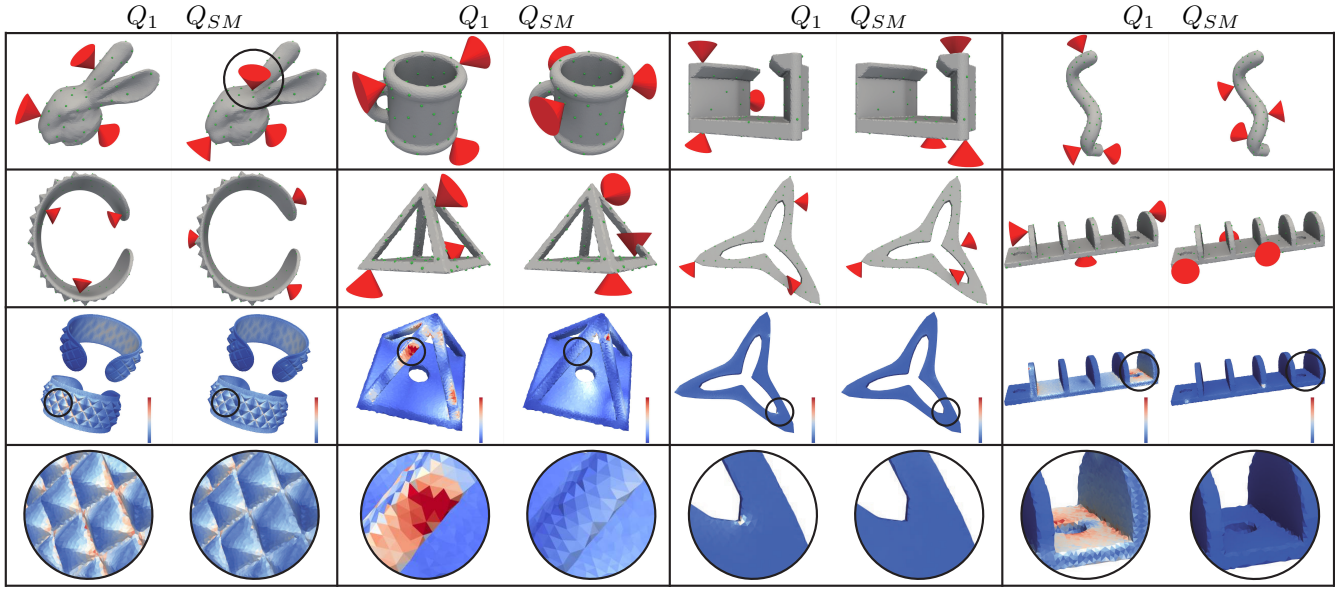


Fig. 4: In the first and second row, we show globally optimal grasps for 8 different target objects under both the Q_{SM} and Q_1 metric. These grasps are generated by choosing $C = 3$ contact points (frictional cones in red) from $N = 100$ potential contact points (green). We choose objects for which optimal grasps are very different under the two metrics. In particular, the optimal grasp for the bunny head object is avoiding the ears of bunny under Q_{SM} metric (black circle). In the third and fourth row, we plot the maximal stress configuration (color coded) for results corresponding to the second row. Using Q_{SM} can drastically reduce the maximal stress as indicated in the black circle.

- [17] V. . Nguyen, "Constructing force-closure grasps," in *Proceedings. 1986 IEEE International Conference on Robotics and Automation*, vol. 3, April 1986, pp. 1368–1373.
- [18] M. A. Roa and R. Suárez, "Grasp quality measures: review and performance," *Autonomous robots*, vol. 38, no. 1, pp. 65–88, 2015.
- [19] J. D. Schulman, K. Goldberg, and P. Abbeel, "Grasping and fixturing as submodular coverage problems," in *Robotics Research*. Springer, 2017, pp. 571–583.
- [20] O. Steinbach, *Numerical approximation methods for elliptic boundary value problems: finite and boundary elements*. Springer Science & Business Media, 2007.
- [21] J. P. Vielma and G. L. Nemhauser, "Modeling disjunctive constraints with a logarithmic number of binary variables and constraints," *Mathematical Programming*, vol. 128, no. 1-2, pp. 49–72, 2011.
- [22] Z. Zhang, J. Gu, and J. Luo, "Evaluation of genetic algorithm on grasp planning optimization for 3d object: A comparison with simulated annealing algorithm," in *2013 IEEE International Symposium on Industrial Electronics*, May 2013, pp. 1–8.
- [23] Y. Zheng, "An efficient algorithm for a grasp quality measure," *IEEE Transactions on Robotics*, vol. 29, no. 2, pp. 579–585, 2012.
- [24] Q. Zhou, J. Panetta, and D. Zorin, "Worst-case structural analysis," *ACM Trans. Graph.*, vol. 32, no. 4, pp. 137:1–137:12, July 2013.

Algorithm 1 Compute upper bound of \bar{Q}_{SM} using [19]

- 1: sample directions $\mathbf{d}_{1,\dots,D}$ in $\text{SO}(3)$
 - 2: **for** $i = 1, \dots, D$ **do**
 - 3: Solve Problem 9 with $\mathbf{d} \leftarrow \mathbf{d}_i$ for \mathbf{w}_i
 - 4: **end for**
 - 5: Return $\min_i \{\mathbf{w}_i^T \sqrt{\mathbb{W}} \mathbf{d}_i\}$
-

APPENDIX

THE BOUNDARY ELEMENT METHOD

In this section, we summarize the boundary element discretization of Equation 2 and the definition of $\mathcal{A}_i, \mathcal{B}_i$. In addition, we derive the special form of BEM with our body force and external traction distribution. We follow [20] with

Algorithm 2 Compute lower bound of \bar{Q}_{SM} using [23]

- 1: sample initial directions $\mathbf{d}_{1,\dots,D}$ in $\text{SO}(3)$
 - 2: **for** $i = 1, \dots, D$ **do**
 - 3: Solve Problem 9 with $\mathbf{d} \leftarrow \mathbf{d}_i$ for \mathbf{w}_i .
 - 4: **end for**
 - 5: $\mathcal{C}_0 \leftarrow \text{ConvexHull}(\mathbf{w}_{1,\dots,D})$
 - 6: Solve Problem 8 with $\mathcal{C} \leftarrow \mathcal{C}_0$ for \bar{Q}_{SM}^0
 - 7: Store the blocking face normal on \mathcal{C}_0 as \mathbf{d}_0
 - 8: **while** $k = 1, \dots$ **do**
 - 9: Solve Problem 9 with $\mathbf{d} \leftarrow \mathbf{d}_{k-1}$ for \mathbf{w}_k
 - 10: $\mathcal{C}_k \leftarrow \text{ConvexHull}(\mathcal{C}_{k-1} \cup \{\mathbf{w}_k\})$
 - 11: Solve Problem 8 with $\mathcal{C} \leftarrow \mathcal{C}_k$ for \bar{Q}_{SM}^k
 - 12: Store the blocking face normal on \mathcal{C}_k as \mathbf{d}_k
 - 13: **if** $|\bar{Q}_{SM}^k - \bar{Q}_{SM}^{k-1}| < \epsilon$ **then**
 - 14: return \bar{Q}_{SM}^k
 - 15: **end if**
 - 16: **end while**
-

minor changes. First, we define a set of notations and useful theorems. For any 3×3 matrix such as $\boldsymbol{\sigma}$, we have:

$$\nabla \cdot \boldsymbol{\sigma} = \begin{pmatrix} \nabla \cdot \boldsymbol{\sigma}_x \\ \nabla \cdot \boldsymbol{\sigma}_y \\ \nabla \cdot \boldsymbol{\sigma}_z \end{pmatrix}.$$

For any 3 vector such as \mathbf{u} , we have:

$$\Delta \mathbf{u} = \nabla \cdot (\nabla \mathbf{u}^T) = \begin{pmatrix} \Delta u_x \\ \Delta u_y \\ \Delta u_z \end{pmatrix}$$

$$\nabla \cdot \nabla \mathbf{u} = \nabla \nabla \cdot \mathbf{u} = \nabla \cdot (\text{tr}(\nabla \mathbf{u}) \mathbf{I}).$$

Algorithm 3 Progressive solve of Problem 9

```

1:  $\mathcal{S} \leftarrow \mathbb{K}$ 
2: while  $\mathcal{S} \neq \{1, \dots, K\}$  do
3:   Solve Problem 10 for  $\mathbf{w}, \mathbf{f}_i, \boldsymbol{\sigma}(\mathbf{x}_j)$ 
4:   Pick  $j^*$  using Equation 11
5:   if  $\sqrt{\|\boldsymbol{\sigma}(\mathbf{x}_{j^*})\boldsymbol{\sigma}(\mathbf{x}_{j^*})\|_2} < 1$  then
6:     Return  $\mathbf{w}, \mathbf{f}_i, \boldsymbol{\sigma}(\mathbf{x}_j)$ 
7:   else
8:      $\mathcal{S} \leftarrow \mathcal{S} \cup \{j^*\}$ 
9:   end if
10: end while
11: Return  $\mathbf{w}, \mathbf{f}_i, \boldsymbol{\sigma}(\mathbf{x}_j)$ 

```

A. Elastostatic Equation in Operator Form

We first derive the operator form of the elastostatic problem. By combining the three equations in Equation 2, we have:

$$\begin{aligned}
0 &= \nabla \cdot (\mu \nabla \mathbf{u} + \mu \nabla \mathbf{u}^T + \lambda \text{tr}(\nabla \mathbf{u}) \mathbf{I}) + \mathbf{g} \\
&= -\mathcal{L}[\mathbf{u}] + \mathbf{g} = \nabla \cdot \boldsymbol{\sigma} + \mathbf{g} \quad (15) \\
\mathcal{L}[\cdot] &\triangleq -(\mu + \lambda) \nabla \nabla \cdot [\cdot] - \mu \Delta [\cdot].
\end{aligned}$$

B. Boundary Integral Equation (BIE)

Next, we derive BIE via the divergence theorem:

$$\begin{aligned}
\int_{\Omega} \mathbf{v}^T \mathbf{g} ds &= \int_{\Omega} \mathbf{v}^T \mathcal{L}[\mathbf{u}] dx = - \int_{\Omega} \mathbf{v}^T \nabla \cdot \boldsymbol{\sigma} dx \\
&= - \int_{\Omega} \nabla \cdot (\boldsymbol{\sigma} \mathbf{v}) dx + \int_{\Omega} \text{tr}(\nabla \mathbf{v} \boldsymbol{\sigma}) dx \\
&= - \int_{\partial \Omega} \mathbf{v}^T \boldsymbol{\sigma} \mathbf{n} ds + \text{Sym}(\mathbf{u}, \mathbf{v}),
\end{aligned}$$

where $\text{Sym}(\mathbf{u}, \mathbf{v})$ denotes a symmetric term in \mathbf{u}, \mathbf{v} satisfying: $\text{Sym}(\mathbf{u}, \mathbf{v}) = \text{Sym}(\mathbf{v}, \mathbf{u})$. We then swap \mathbf{u}, \mathbf{v} and subtract the two equations to get:

$$\begin{aligned}
\int_{\Omega} (\mathbf{u}^T \mathcal{L}[\mathbf{v}] - \mathbf{v}^T \mathcal{L}[\mathbf{u}]) dx &= \int_{\partial \Omega} (\mathbf{v}^T \mathcal{N}[\mathbf{u}] - \mathbf{u}^T \mathcal{N}[\mathbf{v}]) ds \\
\mathcal{N}[\cdot] \triangleq \boldsymbol{\sigma}[\cdot] \mathbf{n} &= \mu \nabla[\cdot] \mathbf{n} + \mu \nabla[\cdot]^T \mathbf{n} + \lambda \nabla \cdot [\cdot] \mathbf{n}. \quad (16)
\end{aligned}$$

C. Fundamental Solution

If \mathbf{v} is the fundamental solution centered at $\tilde{\mathbf{x}}$, which is denoted by $U(\mathbf{x} - \tilde{\mathbf{x}})$, then we have the boundary integral equation by plugging U into Equation 16:

$$\int_{\Omega} U^T \mathbf{g} dx + \int_{\partial \Omega} (U^T \mathcal{N}[\mathbf{u}] - \mathcal{N}[U]^T \mathbf{u}) ds = \mathbf{u}(\tilde{\mathbf{x}}), \quad (17)$$

where the fundamental solution satisfying:

$$\int_{\Omega} \mathcal{L}[U(\mathbf{x} - \tilde{\mathbf{x}})] \mathbf{u}(\mathbf{x}) dx = \mathbf{u}(\tilde{\mathbf{x}}),$$

has the following analytic form:

$$\begin{aligned}
U(\mathbf{x} - \tilde{\mathbf{x}}) &= \frac{1}{8\pi\mu} \left[\Delta r \mathbf{I} - \frac{\lambda + \mu}{\lambda + 2\mu} \nabla^2 r \right] \quad (18) \\
&= \frac{1}{16\pi\mu(1-\nu)r} \left[(3-4\nu)\mathbf{I} + \nabla r \nabla r^T \right] \\
r &\triangleq |\mathbf{x} - \tilde{\mathbf{x}}| \quad \nu = \frac{\lambda}{2(\lambda + \mu)}.
\end{aligned}$$

D. Body Force Term

Equation 17 still involves a volume integral but we can reduce that to surface integral by using the special form of body force: $\mathbf{g}(\mathbf{x}) = \mathbf{g}_0 + \nabla \mathbf{g} \mathbf{x}$ and the Galerkin vector form

of the fundamental solution (Equation 18). The body force term involves two basic terms. The first one is:

$$\begin{aligned}
\int_{\Omega} \Delta r \mathbf{g} dx &= \int_{\Omega} \nabla \cdot (\nabla r \mathbf{g}^T - r \nabla \mathbf{g}^T) dx \\
&= \int_{\partial \Omega} [\mathbf{g} \nabla r^T - r \nabla \mathbf{g}] \mathbf{n} ds.
\end{aligned}$$

The second one is:

$$\begin{aligned}
\int_{\Omega} \nabla^2 r \mathbf{g} dx &= \int_{\Omega} \nabla \cdot (\mathbf{g} \nabla r^T - \text{tr}(\nabla \mathbf{g}) r \mathbf{I}) dx \\
&= \int_{\partial \Omega} [\nabla r \mathbf{g}^T - \text{tr}(\nabla \mathbf{g}) r \mathbf{I}] \mathbf{n} ds.
\end{aligned}$$

Plugging these two terms into Equation 17 and we get:

$$\begin{aligned}
\int_{\Omega} U^T \mathbf{g} dx &= \int_{\partial \Omega} \mathbf{G} \mathbf{n} ds \quad (19) \\
\mathbf{G} &\triangleq \frac{1}{8\pi\mu} \left[(\mathbf{g} \nabla r^T - r \nabla \mathbf{g}) - \frac{\lambda + \mu}{\lambda + 2\mu} (\nabla r \mathbf{g}^T - \text{tr}(\nabla \mathbf{g}) r \mathbf{I}) \right].
\end{aligned}$$

E. Singular Integrals

At this step all the terms in Equation 16 have been transformed into boundary integrals. However, \mathbf{x} in this form must be interior to Ω . In this section, we take the limit of \mathbf{x} to $\partial \Omega$ and derive the Cauchy principle value of singular integral terms.

The first integral in Equation 16, or the body force term in Equation 19, has removable singularity so that we can use numerical techniques to integrate them directly. The second term in Equation 16 takes a special form due to our Dirac external force distribution in Equation 2:

$$\begin{aligned}
\int_{\partial \Omega} U^T \mathcal{N}[\mathbf{u}] ds &= - \int_{\partial \Omega} U^T \sum_{i=1}^N \delta(\mathbf{x} - \mathbf{x}_i) \mathbf{f}_i ds \\
&= - \sum_{i=1}^N U(\mathbf{x}_i - \tilde{\mathbf{x}}^*) \mathbf{f}_i.
\end{aligned}$$

which is also non-singular. The third term in Equation 16 is singular whose value must be determined:

$$\begin{aligned}
&\lim_{\epsilon \rightarrow 0} \int_{\partial \Omega} \mathcal{N}[U]^T \mathbf{u} ds \\
&= \lim_{\epsilon \rightarrow 0} \int_{\partial \Omega - B(\epsilon)} \mathcal{N}[U]^T \mathbf{u} ds + \lim_{\epsilon \rightarrow 0} \int_{\partial \Omega \cap B(\epsilon)} \mathcal{N}[U]^T \mathbf{u} ds,
\end{aligned}$$

where we assume that $\|\tilde{\mathbf{x}} - \tilde{\mathbf{x}}^*\| = \epsilon$, $\tilde{\mathbf{x}}^* \in \partial \Omega$, and $B(\epsilon)$ is the sphere centered at $\tilde{\mathbf{x}}^*$ with radius ϵ . We evaluate the two terms separately. For the first term, we have:

$$\begin{aligned}
&\lim_{\epsilon \rightarrow 0} \int_{\partial \Omega - B(\epsilon)} \mathcal{N}[U]^T \mathbf{u} ds \triangleq \mathcal{D}[\mathbf{u}] \\
&= \int_{\partial \Omega} [2\mu(\mathbb{M}[U])^T \mathbf{u} + (\mathbb{M}[\frac{1}{4\pi r}]) \mathbf{u} + \mathbf{n}^T \nabla[\frac{1}{4\pi r}] \mathbf{u}] ds \\
&= \int_{\partial \Omega} [2\mu U \mathbb{M}[\mathbf{u}] - \frac{1}{4\pi r} \mathbb{M}[\mathbf{u}] + \mathbf{n}^T \nabla[\frac{1}{4\pi r}] \mathbf{u}] ds
\end{aligned}$$

$$\mathbb{M}[\cdot] \triangleq \nabla[\cdot] \mathbf{n}^T - \mathbf{n} \nabla[\cdot]^T,$$

which is known as double layer potential and has only removable singularities. To evaluate the second term, we use the following identity:

$$\begin{aligned}
&\lim_{\epsilon \rightarrow 0} \int_{\partial \Omega \cap B(\epsilon)} \mathcal{N}[U]^T \mathbf{u} ds \quad (20) \\
&= \lim_{\epsilon \rightarrow 0} \int_{\partial(\Omega \cap B(\epsilon))} \mathcal{N}[U]^T \mathbf{u} ds - \lim_{\epsilon \rightarrow 0} \int_{\partial B(\epsilon) \cap \Omega} \mathcal{N}[U]^T \mathbf{u} ds,
\end{aligned}$$

Again, we break this into two terms. The first term in

Equation 20 is easy to evaluate using the divergence theorem:

$$\begin{aligned} & \lim_{\epsilon \rightarrow 0} \int_{\partial(\Omega \cap B(\epsilon))} \mathcal{N}[U_x]^T \mathbf{u} ds \\ &= \lim_{\epsilon \rightarrow 0} \int_{\partial(\Omega \cap B(\epsilon))} \mathbf{n}^T \boldsymbol{\sigma}(U_x)^T \mathbf{u}(\tilde{\mathbf{x}}^*) ds \\ &= -\mathbf{u}(\tilde{\mathbf{x}}^*)^T \lim_{\epsilon \rightarrow 0} \int_{\Omega \cap B(\epsilon)} \mathcal{L}[U_x] ds = -\mathbf{u}_x(\tilde{\mathbf{x}}^*). \end{aligned}$$

The second term in Equation 20 is called the integral free term, which evaluates to:

$$\begin{aligned} & \lim_{\epsilon \rightarrow 0} \int_{\partial B(\epsilon) \cap \Omega} \mathcal{N}[U]^T \mathbf{u} ds \triangleq -\mathbf{C}\mathbf{u} \\ \mathbf{C} & \triangleq \frac{\phi \mathbf{I}}{4\pi} - \int_{\partial(B(\epsilon) \cap \partial\Omega)} (\mathbf{x} - \tilde{\mathbf{x}}^*) \mathbf{n}^T dl, \end{aligned}$$

where ϕ is the internal solid angle at $\tilde{\mathbf{x}}^*$.

F. Putting Everything Together

Plugging all the integrals into Equation 17 and we have:

$$\int_{\partial\Omega} \mathbf{G} \mathbf{n} ds - \sum_{i=1}^N U(\mathbf{x}_i - \tilde{\mathbf{x}}^*) \mathbf{f}_i - \mathcal{D}[\mathbf{u}] = \mathbf{C}\mathbf{u}(\tilde{\mathbf{x}}^*),$$

which is a dense system allowing us to solve for \mathbf{u} every-

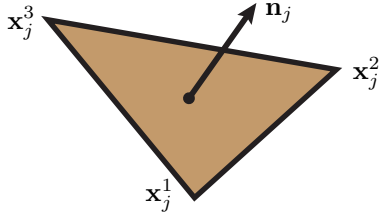


Fig. 5: The j th triangle.

where on $\partial\Omega$. This system is discretized using Galerkin's method with piecewise linear \mathbf{u} and piecewise constant \mathbf{f} . All the integrals are evaluated using variable-order Gauss Quadratures. This linear system is denoted by:

$$(\mathbf{D} + \mathbf{C})\mathbf{u} = \mathbf{A} \begin{pmatrix} \mathbf{g}_0 \\ [\nabla \mathbf{g}]_x \\ [\nabla \mathbf{g}]_y \\ [\nabla \mathbf{g}]_z \end{pmatrix} + \mathbf{B} \begin{pmatrix} \mathbf{f}_1 \\ \vdots \\ \mathbf{f}_N \end{pmatrix},$$

where \mathbf{D} is the coefficient matrix of \mathcal{D} , \mathbf{A} is the coefficient matrix of body force terms, and \mathbf{B} is the coefficient matrix of external force terms. After the displacements \mathbf{u} have been computed, we can recover the stress on j th surface triangle by solving the following linear system:

$$\begin{aligned} \nabla \mathbf{u}_j(\mathbf{x}_j^2 - \mathbf{x}_j^1) &= \mathbf{u}(\mathbf{x}_j^2) - \mathbf{u}(\mathbf{x}_j^1) \\ \nabla \mathbf{u}_j(\mathbf{x}_j^3 - \mathbf{x}_j^1) &= \mathbf{u}(\mathbf{x}_j^3) - \mathbf{u}(\mathbf{x}_j^1) \\ \mu(\nabla \mathbf{u}_j + \nabla \mathbf{u}_j^T) \mathbf{n}_j + \lambda \text{tr}(\nabla \mathbf{u}_j) \mathbf{n}_j &= \mathbf{f}_i \\ \boldsymbol{\sigma}(\mathbf{x}_j) &= \mu(\nabla \mathbf{u}_j + \nabla \mathbf{u}_j^T) + \lambda \text{tr}(\nabla \mathbf{u}_j) \mathbf{I}, \end{aligned} \quad (21)$$

which is 18 linear equations that can be solved for $\nabla \mathbf{u}_j$ and $\boldsymbol{\sigma}(\mathbf{x}_j)$. This linear system is denoted by:

$$\begin{pmatrix} \boldsymbol{\sigma}_x(\mathbf{x}_j) \\ \boldsymbol{\sigma}_y(\mathbf{x}_j) \\ \boldsymbol{\sigma}_z(\mathbf{x}_j) \end{pmatrix} = \mathbf{N}_j \mathbf{u} + \mathbf{M}_j \begin{pmatrix} \mathbf{f}_1 \\ \vdots \\ \mathbf{f}_N \end{pmatrix},$$

where \mathbf{N} , \mathbf{M} are corresponding coefficient matrices in Equation 21. Combining these two systems and we can define $\mathbf{A}_j, \mathbf{B}_j$ as:

$$\begin{aligned} \mathbf{A}_j & \triangleq \mathbf{N}_j (\mathbf{D} + \mathbf{C})^{-1} \mathbf{A} \\ \mathbf{B}_j & \triangleq \mathbf{N}_j (\mathbf{D} + \mathbf{C})^{-1} \mathbf{B} + \mathbf{M}_j. \end{aligned}$$

Algorithm 4 BB algorithm solving Problem 13

```

1: ▷ Each node of the KD-tree is denoted as  $\mathbb{N}$ 
2: ▷ Each  $\mathbb{N}$  is a set and the root  $\mathbb{N}_r = \{1, \dots, N\}$ 
3: ▷ Each internal  $\mathbb{N}$  has two children  $\mathbb{N}_l \cup \mathbb{N}_r = \mathbb{N}$ 
4: ▷ Each  $\mathbb{N}$  with only one element is a leaf node
5: Build a KD-tree for  $N$  contact points
6: ▷ Initialize BB search tree as a queue
7: ▷ Each node in the search tree is a  $C$ -tuple
8: ▷ Each element in the tuple is a node  $\mathbb{N}$ 
9: queue  $\leftarrow \emptyset$ 
10: ▷ Initialize search from the root
11: queue.insert(  $\langle \mathbb{N}_r, \dots, \mathbb{N}_r \rangle$  )
12: ▷ Record the best solution so far
13: best  $\leftarrow \emptyset$  and  $\bar{Q}_{SM}^{best} \leftarrow \infty$ 
14: while queue  $\neq \emptyset$  do
15:     ▷ We use subscript to index KD-tree
16:     ▷ We use superscript to index contact points
17:      $\langle \mathbb{N}^1, \dots, \mathbb{N}^C \rangle \leftarrow$  queue.pop()
18:     Solve Problem 14 with  $\mathcal{S} \leftarrow \mathbb{N}^1 \cup \mathbb{N}^2 \dots \cup \mathbb{N}^C$ 
19:     if  $\bar{Q}_{SM}^{curr} \geq \bar{Q}_{SM}^{best}$  then
20:         ▷ Bound: Stop search early
21:         continue
22:     else
23:         ▷ Check for the last condition in Problem 13
24:         valid  $\leftarrow True$ 
25:         for  $j = 1, \dots, C - 1$  do
26:             if  $\forall a \in \mathbb{N}^j, b \in \mathbb{N}^{j+1}$  we have  $a > b$  then
27:                 valid  $\leftarrow False$ 
28:             end if
29:         end for
30:         if not valid then
31:             continue
32:         end if
33:         ▷ Branch: Desend the KD-tree
34:         isLeaf  $\leftarrow True$ 
35:         for  $j = 1, \dots, C$  do
36:             if  $\mathbb{N}^j$  is not leaf node then
37:                 isLeaf  $\leftarrow False$ 
38:                 queue.insert(  $\langle \mathbb{N}^1, \dots, \mathbb{N}_l^j, \dots, \mathbb{N}^C \rangle$  )
39:                 queue.insert(  $\langle \mathbb{N}^1, \dots, \mathbb{N}_r^j, \dots, \mathbb{N}^C \rangle$  )
40:                 break
41:             end if
42:         end for
43:         ▷ Found a feasible solution
44:         if isLeaf then
45:             best  $\leftarrow \langle \mathbb{N}^1, \dots, \mathbb{N}^C \rangle$  and  $\bar{Q}_{SM}^{best} \leftarrow \bar{Q}_{SM}^{curr}$ 
46:         end if
47:         end if
48:     end while
49: for  $j = 1, \dots, C$  and  $i = 1, \dots, N$  do
50:     if  $i \in \mathbb{N}^j$  then
51:          $z_i^j \leftarrow 1$ 
52:     else
53:          $z_i^j \leftarrow 0$ 
54:     end if
55: end for

```
